

Modeling, assessment and characterization of soiling on PV Technologies. Toward a Better understanding of the Relation between dust deposition and performance losses

Maryam Mehdi^a, Ricardo Conceição^{b,*}, Nabil Ammari^a, Ahmed Alami Merrouni^{a,*}, José González-Aguilar^b, Mohamed Dahmani^a

^a Materials Science, New Energies, and Applications Research Group, LPTPME Laboratory, Department of Physics, Faculty of Sciences, Mohammed 1st, University, 60000 Oujda, Morocco

^b High Temperature Processes Unit, IMDEA Energy, Avda. Ramón de la Sagra 3, 28935 Móstoles, Spain

ARTICLE INFO

Keywords:

Soiling
Modeling and monitoring
Outdoor microscopy system
Dust composition
Semi-arid climate

ABSTRACT

Soiling is a critical, site-specific challenge that affects the performance and economic viability of photovoltaic power plants. This study evaluates the effectiveness of an outdoor microscopy method under the specific climatic conditions and dust composition of the Mid-south region of Morocco. Semi-empirical models were developed to correlate the Soiling Coverage Index with losses in optical and electrical performance. Additionally, a comprehensive analysis of local dust, encompassing its chemical composition, morphology, and size distribution, was conducted. Results indicate quartz as the predominant mineral in Benguerir city's dust particles, with diameters ranging from 0 μm to 26 μm . Additionally, following a 2-week exposure with no rainfall, a dust density of 2.5 g/m² accumulated on the deployed glass coupons, resulting in a soiling ratio of 6.9 % and a relative transmittance loss of 15.19 %. The surface coverage index, as calculated by the outdoor microscope, was 9.16 %. Furthermore, the evaluation of this metric revealed strong positive correlations ($r^2 = 0.95$ to 0.99) with key soiling indicators such as dust density, soiling ratio, and transmittance loss. These findings underscore the efficacy of the outdoor microscope as a fast, low-cost, and reliable soiling monitoring sensor, offering valuable insights for future monitoring and mitigation efforts.

Introduction

Solar technologies, particularly photovoltaics, are significant contributors to clean energy production, especially in sun-belt regions with abundant solar resources [1]. However, these areas often experience high levels of airborne dust, leading to increased soiling on PV panels, which lowers their efficiency and power output [2,3]. Soiling phenomenon, defined as the deposition of dust, dirt, and contaminants on PV modules, causes power output degradation by reducing the energy received by the semiconductor through absorption and scattering of the incoming solar radiation [4,5]. Its adverse impact on PV panel efficiency is substantial, surpassing 1 %/day power reduction, making it the third most influential factor determining panel productivity after irradiance and temperature [6,7]. Zaihidee *et al.* emphasized the negative impact of deposited dust, noting that a dust density of 20 g/m² could produce a degradation of 15–21 % in short circuit current, 2–6 % in open circuit

voltage, and 15–35 % in overall efficiency [8]. Said *et al.* conducted an outdoor experiment in Dhahran, KSA, revealing a significant impact of soiling on the short circuit current of the PV modules, resulting in an average reduction of 13 %, causing an overall power drop of 6 % after 5 weeks of exposure [9]. Conceição *et al.* have noted in their comprehensive review that soiling rates in dry climates can range from 0.1 % to 1 % per day for PV systems, reducing global solar power production by 3 %–7 % [10].

Fortunately, soiling is reversible through cleaning, which restores the electrical and optical performance of PV panels. However, regular manual or automated cleaning can lead to high operational and maintenance (O&M) expenses, increasing the levelized cost of electricity (LCOE) [2]. Given the need for optimized cleaning schedules to maximize profits, effective soiling monitoring and assessment is crucial [11]. Various measurement setups and sensors are used for evaluating soiling on PV modules, generally falling into two main categories: electrical and optical [13,14]. The first category relies on the direct measurement of

* Corresponding authors.

E-mail addresses: ricardo.conceicao@imdea.org (R. Conceição), alami.univ.oujda@gmail.com (A. Alami Merrouni).

<https://doi.org/10.1016/j.seta.2024.104023>

Received 7 June 2024; Received in revised form 28 August 2024; Accepted 11 October 2024

Available online 14 October 2024

2213-1388/© 2024 Elsevier Ltd. All rights are reserved, including those for text and data mining, AI training, and similar technologies.

Nomenclature		r^2	Coefficient of determination
A	Area of glass coupon [m ²]	RH	Relative Humidity [%]
d_{dust}	Dust density [g/m ²]	RMSE	Root Mean Squared Error
DHI	Diffuse Horizontal Irradiation [W/m ²]	SCI	Surface Coverage Index [%]
DNI	Direct Normal Irradiation [W/m ²]	SEE	Sum of Squared Errors
GHI	Global Horizontal Irradiation [W/m ²]	SEM	Scanning Electron Microscopy
Isc	Short circuit current [A]	SR	Soiling Ratio [%]
m	Dust mass [g]	Ta	Ambient Temperature [°C]
MAE	Mean Absolute Error	Tdew	Dew temperature [°C]
MSE	Mean Squared Error	WS	Wind Speed [m/s]
OSM	Outdoor Soiling Microscope	XRD	X-ray Diffraction
PV	Photovoltaic	τ_l	Relative transmittance loss [%]

electrical loss resulting from dust accumulation on the panel surface. Soiling stations, which are the prominent setup in this class, require a simple setup consisting on the installation of two identical PV modules side by side with one regularly cleaned and the other left to accumulate natural soiling. Performance loss is then assessed using the soiling ratio (SR) metric derived from electrical measurements of both panels [12]. The optical category quantifies soiling loss indirectly through changes in the optical properties of the surface. Mars and DustIQ were the first commercial optical soiling monitors [13]. Kipp&Zonen’s DustIQ measures soiling loss by evaluating the drop in transmittance of a soiled window using a monochromatic light source and an integrated photodiode [14,15]. The Mars sensor, developed by Atonometrics, uses a digital camera to capture images and estimate transmittance drop from the brightness of the soiled window [16,17]. Recently, researchers from the University of Jaén in Spain and the National Renewable Energy Laboratory (NREL) in USA introduced the DUSST sensor, which measures soiling losses by emitting monochromatic light onto a soiled glass coupon and comparing the transmitted light to clean reference conditions [18,19]. These soiling monitoring sensors assume a uniform transmittance profile across the light spectrum. However, soiling spectral transmittance varies across wavelengths, leading to potential measurement inaccuracies. Additionally, different PV materials respond differently to soiling, further complicating the assessment process [20].

Imaging techniques are widely used to understand and quantify soiling phenomena, providing insights into the size, arrangement, and distribution of soiling particles on surfaces. Kassab *et al.* investigated the detachment of micrometer-sized particles from various surfaces using a high-speed camera in a wind tunnel [21]. Similarly, Biryukov *et al.* developed a computerized microscope system for examining the adhesion of dust particles to the surface of solar collectors in laboratory conditions [22]. Recently, the affordability and improved capabilities of cameras have led to an increase in on-site soiling characterization using camera imaging. Figgis *et al.* introduced a cost-effective method for evaluating dust accumulation and removal on transparent surfaces using outdoor imaging techniques [23]. Their setup, involving a compact digital microscope to capture images of soiling on a glass coupon’s rear surface, aims to correlate meteorological variables with dust accumulation. Recorded images were post-processed using ImageJ software to calculate the surface coverage [24].

Since dust composition differs from one location to another, the first objective of the current investigation is to assess the effectiveness of the Outdoor Soiling Microscope (OSM) as a monitoring sensor for soiling in the semi-arid climate in the mid-south region of Morocco. This comprehensive study was based on a multifaceted methodology involving the realization, test, and validation of the OSM setup by comparing its surface coverage index (SCI) with data from conventional techniques for soiling quantification: electrical measurement (soiling ratio), optical measurement (transmittance loss) and dust density analysis. The novelty of this study lies in the development of semi-empirical models enabling

Table 1
Measuring sensors uncertainties.

Sensor	Measured parameter	Uncertainty
CHP1 pyrheliometer	DNI	±1%
CMP21 pyranometer	DHI & GHI	±2%
Campbell CS215	Ta & RH	±0.4 %
NRG 40C anemometer	Wind speed	<0.1 m/s
NRG 200P wind vane	Wind direction	<1%

the prediction of soiling loss by linking these parameters with the SCI, integrating empirical findings from experimental data with theoretical insights into the mechanisms underlying the soiling phenomenon. Additionally, the current study includes a detailed background analysis of local dust particles, examining their chemical composition, morphology and size, which is a critical process in understanding soiling behavior and developing empirical models.

The paper is structured as follows. Section 2 presents the experimental setup and the methodology used. Section 3 is dedicated to present the obtained result. First, a glance at the meteorological conditions throughout the experiment, followed by the detailed analysis and characterization of local dust. Afterwards, the evaluation and validation of the OSM setup results are presented. Key results of this study are provided in the conclusion section.

Materials and methods

Location and Environmental parameters assessment

This work was conducted at the Green Energy Park (GEP) Research Facility in Benguerir, located in the mid-south of Morocco. This site belongs to BSh category according to the Köppen climate classification and it is characterized by a hot semi-arid climate with a dry and hot summer and cold winters with low precipitation. GEP possesses a substantial solar resource with an annual global horizontal irradiance availability (GHI) of 2239 kWh/m², which makes it an appealing site for the deployment of solar technologies. A meteorological station equipped with high-precision sensors was strategically positioned within the study area to record and evaluate weather conditions. Ambient temperature and relative humidity were continuously monitored by a Campbell CS215 sensor, and wind speed and direction were assessed with an NRG 40C anemometer and NRG 200P wind vane, respectively. Solar irradiation components, such as direct normal irradiance (DNI), diffuse horizontal irradiance (DHI), and global horizontal irradiance were measured using a CHP1 pyrheliometer and CMP21 pyranometer from Kipp&Zonnen. Table 1 lists the accuracy of different sensors. This equipment allowed for recorded meteorological parameters at a frequency of 10 s, and the data were averaged afterwards to 1-minute step.



Fig. 1. Outdoor soiling assessment experimental setup and laboratory measuring equipment: (Top left) Outdoor Soiling Microscope; (Top right) Soiling measuring station; (Bottom left) JSM-7900F field emission Scanning Electron Microscope used for the characterization of dust shape, morphology, and size; and (Bottom right) Microbalance utilized for the measurement of accumulated dust mass.

Given the impact of dew on particle adhesion, it was of key importance to assess it during the experimental period. This phenomenon is defined as the formation of water droplets resulting from water vapor condensation on a cold surface. The formation of water droplets on soiled PV surfaces results in the rearrangement and entrapment of dust particles, enhancing adhesion forces [25]. Dew point temperature was assessed by measuring the PV module temperature using a PT1000 platinum temperature sensor attached to its rear surface. Subsequently, dew point temperature was theoretically calculated using the Magnus formula [26], as in equation (1):

$$T_{dew} = \frac{c}{b - \left[\ln\left(\frac{RH}{100}\right) + \frac{bT}{c+T} \right]} \left[\ln\left(\frac{RH}{100}\right) + \frac{bT}{c+T} \right], \quad (1)$$

where $b = 17.67$ and $c = 243.5^\circ\text{C}$, which correspond to the Magnus parameters, RH is the relative humidity (in %) and T is the ambient temperature (in $^\circ\text{C}$).

Experimental setup

To quantify the extent of soiling and evaluate the performance of the Outdoor Soiling Microscope (OSM), three simultaneous outdoor experiments were conducted at GEP from June 16 to June 29, 2023 (a period of two weeks). The first experiment focused on the calculating the

Soiling Coverage Index (SCI) using the OSM. The second experiment measured soiling using electrical parameters extracted from the soiling station, which involved two photovoltaic (PV) modules, one kept clean and the other exposed to dust accumulation, see Fig. 1. The third experiment aimed to assess soiling from an optical perspective by exposing glass samples, close by the OSM setup, to monitor the drop in transmittance and to analyze the characteristics of dust particles accumulated on the glass surfaces. More details about the materials used and the experimental protocols are listed below.

Outdoor soiling microscope setup

The OSM principle consists of monitoring the rear surface of an exposed coupon made of photovoltaic glass ($5 \times 5 \text{ cm}^2$) by means of a 5 V compact digital microscope. The microscope employed in this study is capable of capturing images at a rate of 20 frames per second under illumination of 500 lx provided by 8 built-in LED lamps. Additionally, it offers a magnification of 1600X and automatically records images with a resolution of 640x480 pixels when connected to a Raspberry Pi electronic component. The digital microscope as well as the necessary electronics for its operation, were installed in an aluminum enclosure to safeguard against atmospheric conditions such as wind, dew or precipitation. The current OSM setup has been designed to track up to four samples at the same time. Furthermore, in order to ensure a suitable quality of recorded images, a 12 W LED light source and a light diffuser (made of rectangular regular translucent paper) were positioned in front

of the glass samples and produced a homogeneous illumination, while the built-in LED lamps of the microscope were turned off. The entire setup was tilted 31° south, which corresponds to the optimal angle for stand photovoltaic modules installed at the region. It is worth noting that this configuration closely resembles the system described in [23].

Soiling station setup

The second experiment was performed using soiling station to have a reference and standardized method of quantifying soiling. To this end, two identical 255 W_p polycrystalline PV modules were installed at the GEP testing field, south-oriented and also tilted 31°. One of the panels was cleaned every day, while the other was left to naturally get soiled. Electrical parameters, such as short circuit current (I_{sc}), open circuit voltage (V_{oc}), maximum power (P_{mpp}), maximum power point voltage (V_{mpp}), and maximum power point current (I_{mpp}) of both panels were continuously measured with a 10-second frequency using an ISET®-MPP from Sol. Connect. This data logging system is a dual-monitoring device that can handle two PV modules simultaneously with a capacity of 300 W and a maximum current of 12.5 A each. The ISET®-MPP data logger is well-suited for outdoor testing, as it can handle operating temperatures in the range of −10 to + 50 °C. It offers a (U, I) measurement resolution of 16 bits and an accuracy of less than 1 % for voltage and current. It can also capture up to 256 data points for the current–voltage characteristic curve within a 320 ms measurement period. In the present study, the ISET®-MPP datalogger was linked to a SCADA system for the storage of all measured data.

Glass transmittance setup

The third experiment consisted in exposing 14 glass samples of 5 cm² for different time spans. Samples were installed in the same testing field and carefully fixed on an open rack facing south, tilted 31°, and approximately elevated by 1 m from the ground level. On each day of the experiment, one sample was selected for retrieval, generating a set of samples with exposure periods ranging from one to 14 days. Samples were then stored in airtight boxes to preserve the dust configuration on the surfaces.

Soiling quantification methodology

OSM image analysis

The Outdoor Soiling Microscope was set to capture images every 10 min, producing 144 images per day. To ensure data representativeness, only images taken under clear skies between 11 AM and 2 PM were analyzed. This time frame was chosen because it corresponds to the period when irradiance is more stable and PV angular dependence is lower. Additionally, it aligns with the calculation period for the soiling ratio (SR), which will be correlated with the surface coverage index derived from these images. A MATLAB-based image analysis code was developed to examine the particles identified by the OSM. Images were initially captured in RGB format and later converted to grayscale.

It was challenging to retrieve particles from the initial images due to insufficient contrast, leading to potential detection errors. To address this, contrast adjustment was applied to all grayscale images using an empirically determined saturation interval between 0.2 and 0.7. Despite this adjustment, small particles remained difficult to identify during binarization, and some unwanted blurriness persisted. To improve particle visibility, image sharpening was performed using a low-pass Gaussian filter with a standard deviation of 2. Subsequently, adaptive binarization was applied, assuming black particles on a white background, with a sensitivity of 0.55. Besides, artifacts 1 pixel in size due to camera resolution and image manipulation were removed. Afterward, the surface coverage index was calculated as a ratio in the percentage of the summation of black pixels in an image and its total area as follows in equation (2):

$$SCI_i = 100 \frac{\sum b_i}{A_i}, \quad (2)$$

where b_i corresponds to the black pixels of image i and A_i to the total area in pixels of the corresponding image.

Transmittance drop and dust density measurements

To establish a comprehensive comparison with the OSM results, two other conventional methods were employed: transmittance and dust density measurements, corresponding to the second setup. For determining the accumulated dust density, each glass coupon underwent weighing before and after exposure, using a microbalance from KERN® with a precision of 0.0001 g. Final dust density values, d_{dust} , in g/m² were calculated by subtracting the mass after exposure, m_s , from the initial clean state, m_c , and dividing the result by the total area of the glasses, A , as it follows in equation (3):

$$d_{dust} = \frac{m_s - m_c}{A} \quad (3)$$

Following the dust density measurements, seven glass samples representing different exposure periods were selected for transmittance evaluation along a clean reference, while the other coupons were separately derived to undergo scanning electron microscopy (SEM) analysis. Measurements were performed using a LAMBDA 1050 UV/Vis Spectrophotometer PerkinElmer®, offering a wide wavelength range from Ultraviolet (UV) to Near-infrared (NIR). Spectral transmittance was measured for the wavelength interval between 300 nm and 1200 nm with a 1 nm step. Direct transmittance loss, τ_l , expressed as a percentage, was utilized to quantify the portion of incident light transmitted through the glass sample. It is worth noting that, to mitigate the impact of non-uniform dust distribution on the glass surface, transmittance was measured at two different points on each sample. The desired value was then determined as the average of these two measurements. Finally, transmittance loss was subsequently calculated as in equation (4) [27]:

$$\tau_l = 100 \frac{\sum_{\lambda} [\tau_c(\lambda) - \tau_s(\lambda)]}{\sum_{\lambda} \tau_c(\lambda)} \quad (4)$$

where τ_c is the transmittance of the reference clean glass sample (%) and τ_s corresponds to the transmittance of the soiled glass sample (%).

Soiling metric

Regarding the third experimental setup, data was analyzed and grouped into sets with a temporal resolution of one hour. To evaluate the daily soiling effect, the percentage drop in electrical short-circuit intensity of the soiled module when compared to the clean module, was calculated specifically around solar noon (from 11 AM to 2 PM), corresponding to the period where irradiance is more stable and PV angular dependence is lower [28]. The calculation of the latter was performed as follows in equation (5):

$$SR = 100 \frac{\sum_{t_i}^t [I_{sc_c}(t) - I_{sc_s}(t)]}{\sum_{t_i}^t I_{sc_c}(t)} \quad (5)$$

where I_{sc_s} corresponds to the short circuit current of the soiled PV module and I_{sc_c} is the short circuit current of the clean PV module. t_i and t_f delineate the temporal range over which the summation operation is executed, encompassing all values of the short circuit current around solar noon (from $t_i = 11$ AM to $t_f = 2$ PM).

Dust characterization

To analyze the local dust nature and properties, two distinct methods were utilized at IMDEA Energy. Mineral and chemical composition was determined by X-ray diffraction (XRD), a process that entailed collecting bulk dust samples from the surface of a soiled PV panel installed at GEP.



Fig. 2. Daily variation of meteorological data. (Top) air temperature; (center) Relative humidity; and (bottom) Wind speed.

Afterward, the samples underwent a detailed analysis using a Bruker D8 Advance diffractometer with accuracy ($\leq 0.01^\circ 2\theta$) in terms of peak position, intensities, and resolution. Outputs were then examined with X'Pert HighScore Plus software. Simultaneously, for a closer examination of the dust particles' shape, SEM analysis was employed. This involved selecting some of the dusty glass samples exposed during the experiment and subjecting them to microanalysis using a JSM-7900F field emission SEM, from Jeol (see Fig. 1). These combined methods allowed for a comprehensive study, providing insights into both the chemical composition and physical characteristics of the dust at the site under study.

Furthermore, particle size distribution was obtained by image processing using ImageJ software. To avoid particle agglomeration, that can significantly affect the particle's diameter measurement, SEM images captured at the beginning of the exposure experiment were selected to be analyzed. Upon importing the SEM images into ImageJ, images were converted to 8-bit grayscale to enhance contrast, followed by thresholding to distinguish particles from the background. Particular attention was given to setting the circularity parameter within a range of 0.5 to 1.0, allowing the analysis and count of particles that are moderately to perfectly circular. This circularity range was selected to balance the exclusion of highly irregular shapes that could represent non-particle

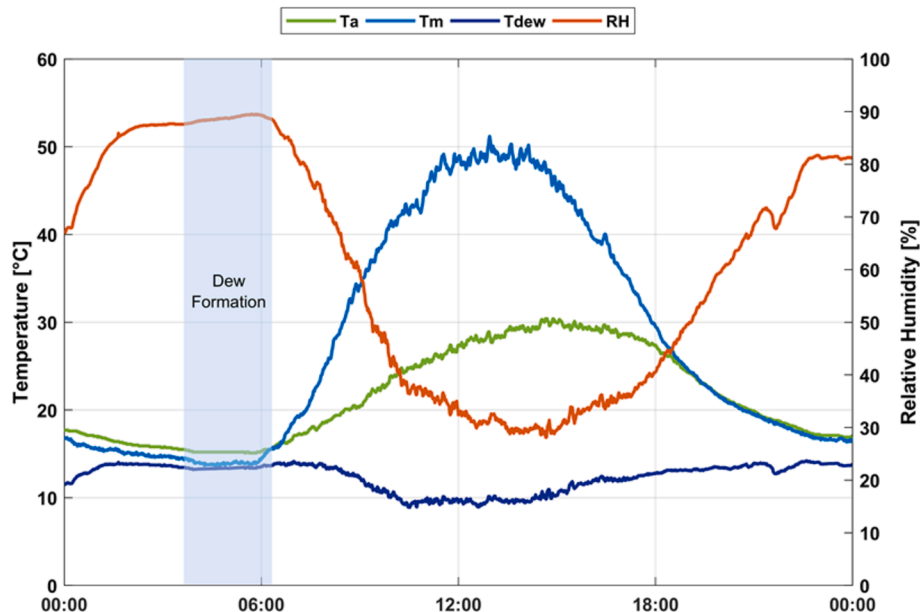


Fig. 3. Ambient and PV module temperature, relative humidity, and dew temperature on June 29th 2023.

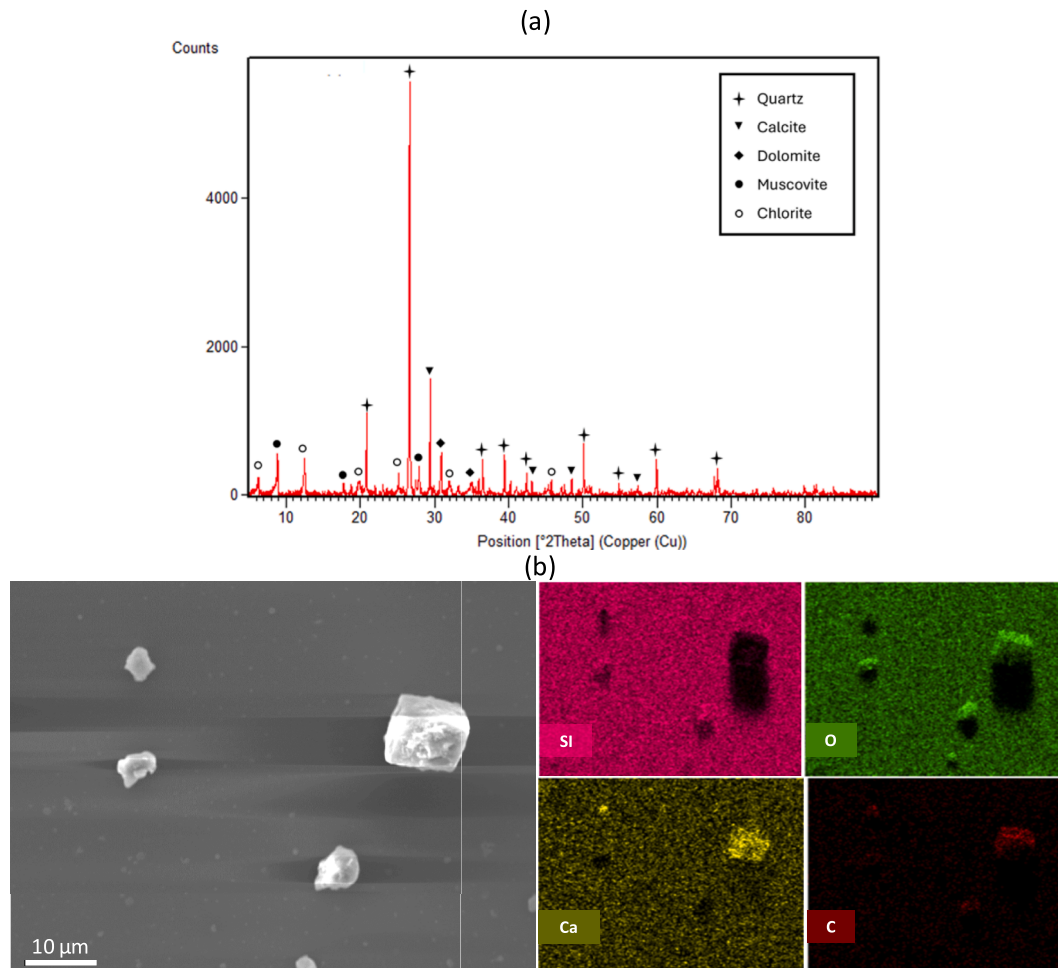


Fig. 4. (a) X-ray diffractogram of dust collected from a PV module surface in the exposure site along with the morphological and chemical composition characterization (b left) SEM micrograph; and (b right) EDX images.

entities. Subsequently, the equivalent circular diameter, which provides a standardized basis for comparing particle sizes, regardless of irregularities in particles' shape, was calculated for each particle. This parameter was derived from the particle's area (A) assuming that this later is equal to the area of an idealized circle, as demonstrated in equation (6):

$$d = 2\sqrt{A/\pi} \quad (6)$$

Results and Discussion

Environmental parameters

Meteorological parameters are of greatest influence on soiling, mainly atmospheric particulate matter, dew, precipitation, ambient temperature, relative humidity (RH), and wind speed [29]. Daily-averaged ambient temperature, relative humidity, and wind speed throughout the experimental period are represented in Fig. 2. Daily-averaged mean ambient temperature exhibited variations around 22 °C, with daily maxima reaching up to 35 °C at the experiment onset and exceeding 28 °C for the remaining period. Besides, relative humidity depicted a distinct pattern, with high average values varying around 59 %. During nights and early mornings, RH surged beyond 80 % while it experienced a significant decrease throughout the day, dropping to values lower than 30 %. Wind speed emerged as a noteworthy factor, registering relatively high values with a daily average of up to 4 m/s. This elevated average can be attributed to the occurrence of wind gusts,

reaching speeds around 7 m/s while occasionally surpassing 8 m/s.

Examination of meteorological parameters during the experiment unveiled a notable propensity for dew formation. Assessment of dew point temperature in conjunction with PV module temperature consistently revealed the recurring incidence of dew throughout the experimental period. For a more nuanced understanding, Fig. 3 illustrates ambient and PV module temperature, relative humidity, and calculated dew temperature as function of time on June 29th. During late night and early morning hours, relative humidity surpasses 88 % and the module temperature decreases and becomes close to dew temperature primarily due to radiative cooling. Thus, this analysis points out dew formation between 4 AM to 6 AM. This meteorological analysis suggests that the site's conditions are favoring dew formation in the early mornings which could contribute to higher soiling rates by increasing particulate adhesion. Therefore, a thorough assessment and continuous monitoring of soiling phenomenon is essential to sustain the optimal plants' performance under such circumstances.

Dust characterization

Mineral, morphological and chemical composition analyses of dust collected at Benguerir were performed by XRD, SEM, and Energy-Dispersive X-Ray Spectroscopy (EDX). Diffractogram, which is shown in Fig. 4(a), reveals the presence of quartz (SiO_2), calcite (CaCO_3), dolomite ($\text{Ca}_3\text{Mg}_3\text{C}_6\text{O}_{18}$), chlorite ($(\text{Mg,Fe,Al})_6(\text{Si,Al})_4\text{O}_{10}(\text{OH})_8$), and muscovite ($\text{KAl}_2(\text{Si}_3\text{Al})\text{O}_{10}(\text{OH})_2$). Quartz emerged as the predominant mineral, displaying robust and distinct peaks, followed by calcite and

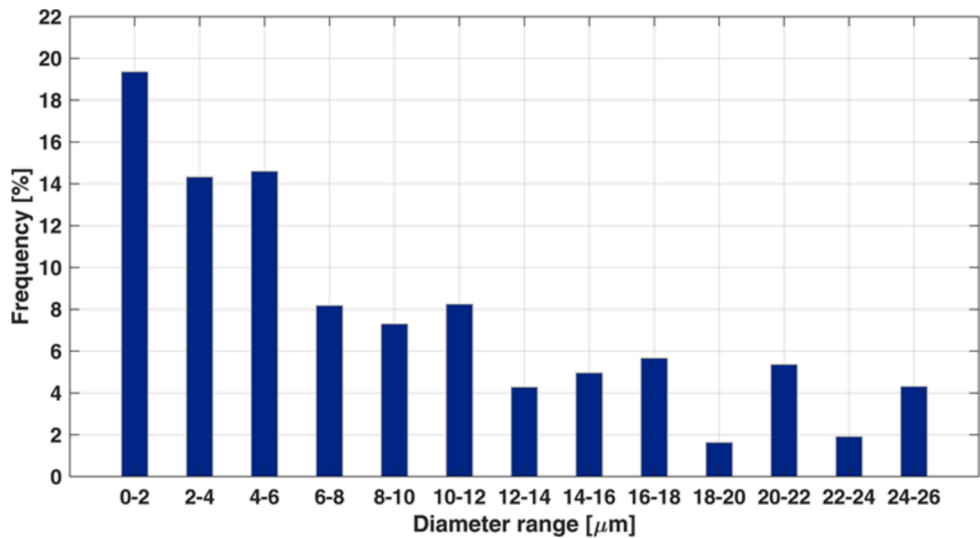


Fig. 5. Particle size distribution obtained by analyzing SEM micrographs.

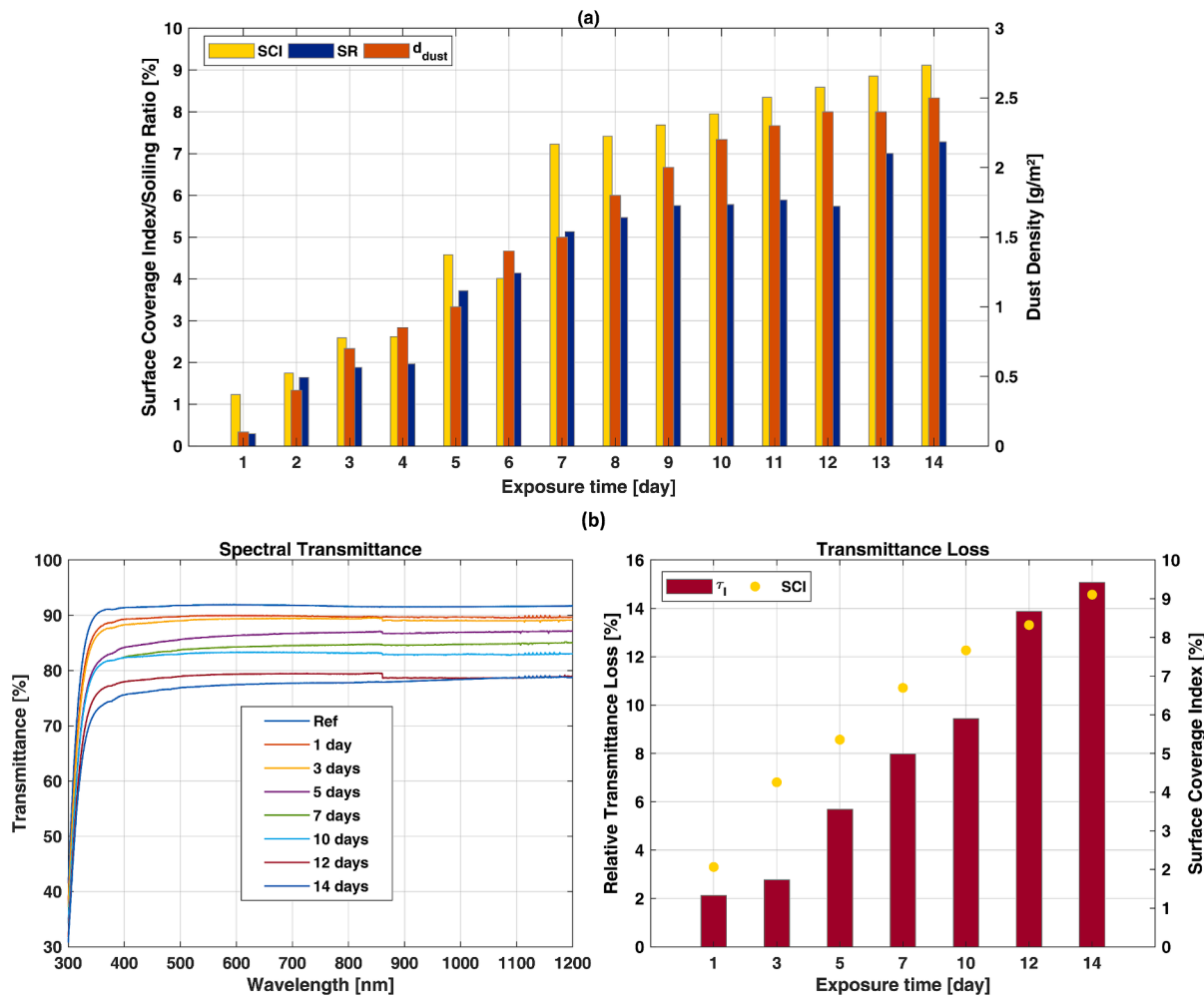


Fig. 6. (a) Soiling ratio throughout the experimental period shown together with surface coverage index and dust density;(b) Optical loss throughout the exposure days: (left) Transmittance vs wavelength; and (right) Associated relative transmittance loss and surface coverage index with time.

dolomite. SEM micrographs shown in Fig. 4(b) point out that dust particles have diverse sizes and irregular morphologies, reflecting the varied elements identified before in the XRD analysis. Besides EDX indicates

an abundance of Silicon (Si), Oxygen (O), Calcium (Ca), and Carbon (C). Silicon presence is attributed to soil erosion and anthropogenic activities, while the occurrence of Calcium can be linked to emissions related

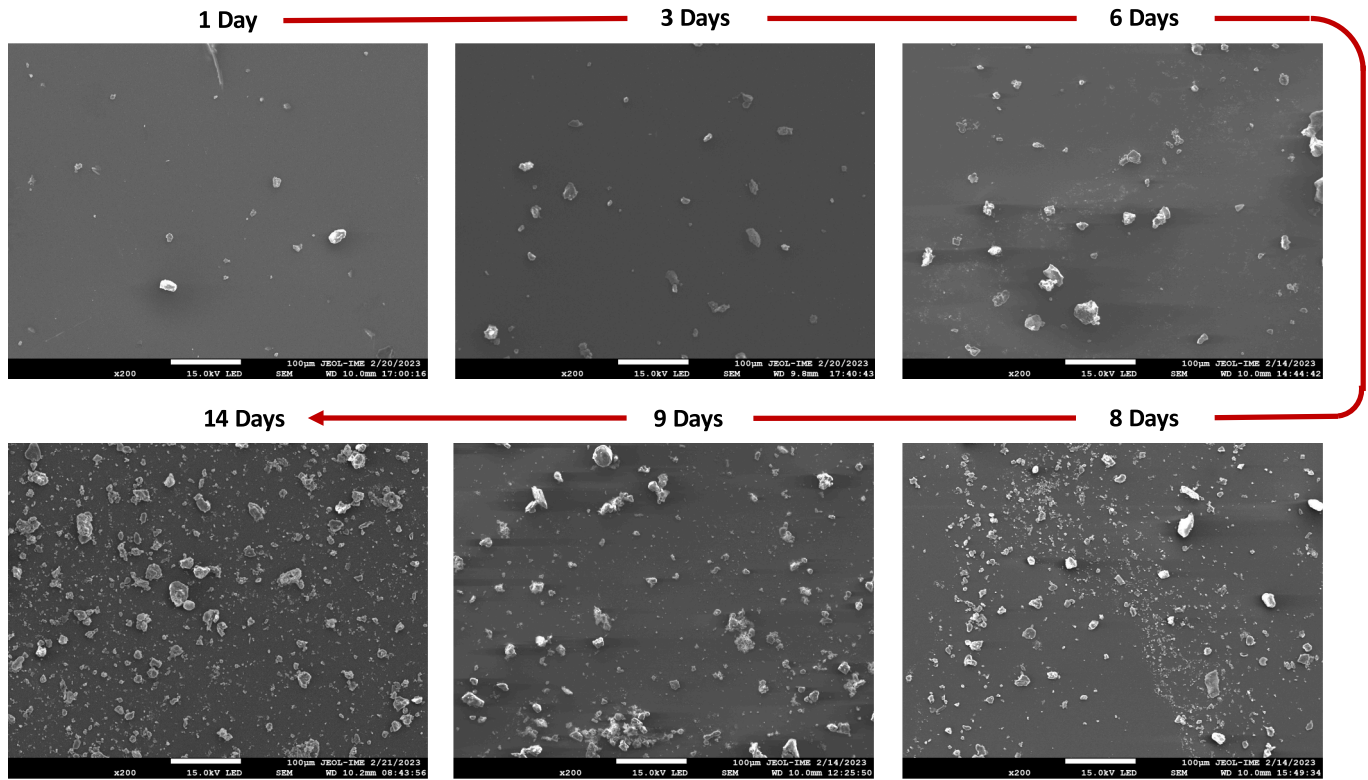


Fig. 7. SEM images of the exposed glass samples with a 200x magnification for different accumulation periods.

to construction works [30].

Analysis of dust particle size resulted in the histogram showcased in Fig. 5. A frequency of 19.35 % was observed within the ultrafine particle range 0–2 μm which could be linked to natural processes, such as soil erosion and wind-blown sand that characterize climate and anthropogenic activities at Benguerir. These potentially include agriculture and traffic, which are known to generate fine particulate matter. These small particles are reported to cause higher optical losses for the same density of larger deposited dust [31]. Moreover, the silt-sized particles, expected to be abundant in arid and semi-arid regions as previously stated in several studies [2], are indeed well-represented in the histogram in which more than 80 % of particle diameter is between 2 μm and 26 μm . Frequencies of 14.32 % and 14.56 % are observed in the ranges from 2 to 4 μm and from 4 to 6 μm , respectively. In addition, larger particles with diameters in the range between 20 and 26 μm are present in the analyzed dust with a total frequency of 11.56 %.

Soiling assessment

As mentioned in Section 2, four different methodologies for soiling quantification were used to monitor soiling and evaluate the OSM setup. These included measuring the surface coverage index using the OSM images, determining soiling dust density, assessing the soiling ratio through electrical measurements from a dedicated soiling station, and calculating the relative transmittance loss (τ_i) based on optical measurements taken from exposed glass samples. Fig. 6(a) gathers the results from the first three methods, while Fig. 6(b) plot the relative transmittance loss in conjunction with the variation of the spectral transmittance of each glass sample. Upon examination of Fig. 6(a), it is observed that the surface coverage index, dust density, and soiling ratio exhibit relatively similar responses to soiling accumulation, showcasing a consistent upward trend over the experiment days. The initial dust density of 0.099 g/m² at the experiment's beginning experienced a gradual increase with an average relative value of 6.86 %/day and reached 2.5 g/m² on the 14th exposure day. Consequently, this final

deposited dust resulted in a surface coverage index of 9.11 % and a corresponding soiling ratio of 7.28 %.

Similar to the patterns observed in the investigated parameters, relative transmittance demonstrates a consistent decreasing trend from 91.66 % to 77.73 %. This decrease corresponds to a total relative transmittance loss of 15.19 % after two weeks of outdoor exposure. Moreover, it is observed in Fig. 6(b) that the increasing trend of relative transmittance losses is in accordance with that of the surface coverage index, suggesting their similarity regarding the response to dust accumulation. It is noteworthy to emphasize that no rainfall events were recorded throughout the entire experimental period. The absence of precipitation resulted in excessive accumulation of dust particles, explaining the observed increasing trend in almost all the evaluated soiling indicators.

Additionally, an examination of the microstructure detailing the evolution of soiling during the experiment was conducted using SEM micrographs at 200x magnification, as illustrated in Fig. 7. Images distinctly reveal that during the initial days of exposure (1st – 3rd day), there is a dispersed accumulation of relatively few dust particles exhibiting varied shapes and sizes, ranging from approximately 1 μm to 20 μm in diameter. As of the 6th day, a noticeable shift occurs, with smaller dust particles featuring diameters in the nanometer range appearing alongside larger particles on the glass coupon surface. The distribution of these nanometric particles seems to delineate paths created by water droplets resulting from dew formation during early morning hours, subsequently evaporating as the ambient temperature rises throughout the day. Dew might not only enhance the adhesion forces of particles already accumulated at the surface before dew happens, but also easily traps new particles. Following 8 days of exposure until the end of the experiment, a noticeable transformation is observed in the dust particles arrangement, manifesting in more confined and agglomerated patterns. This configuration highlights the strength of adhesion forces, making soiling removal harder.

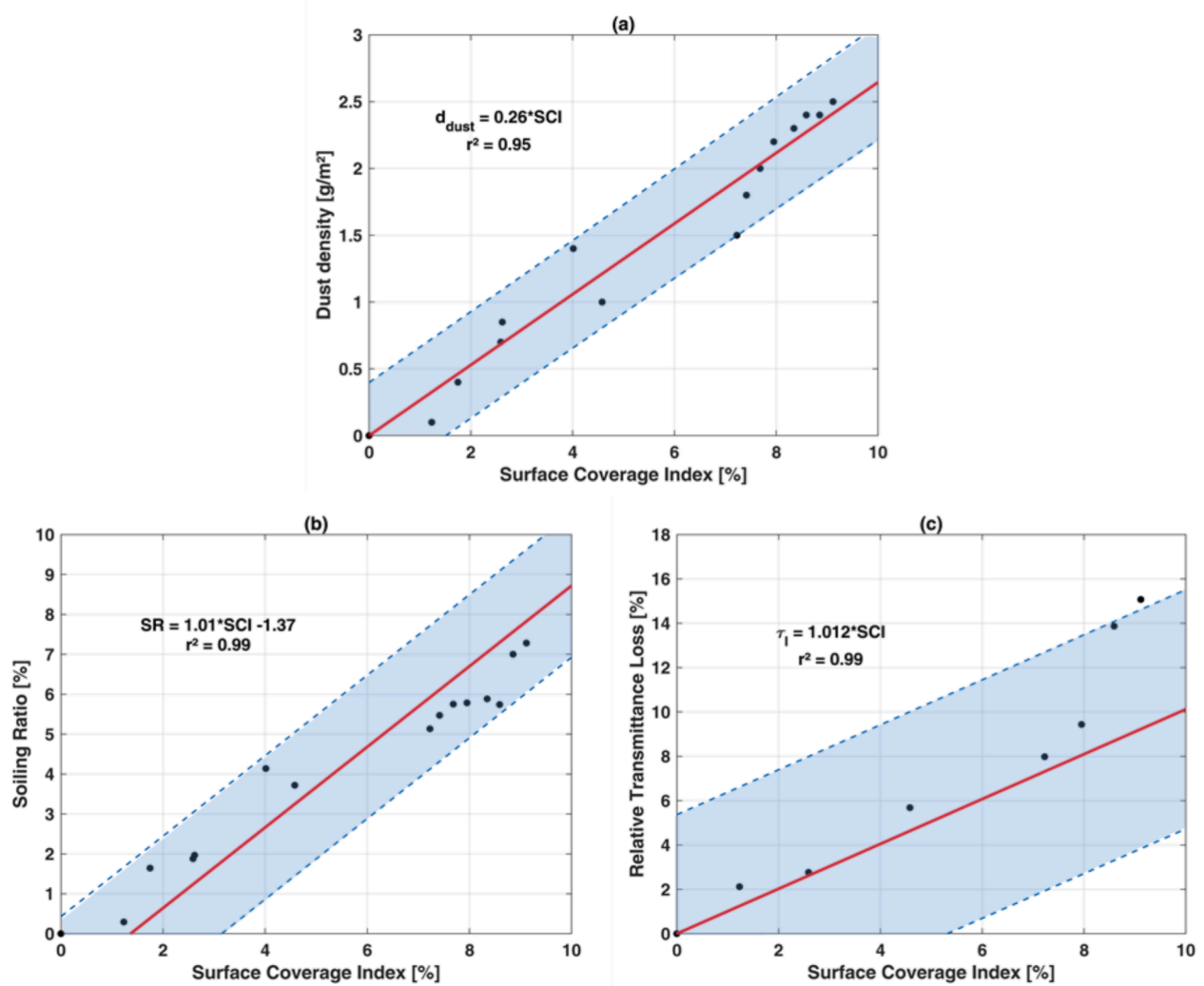


Fig. 8. Correlation between Surface Coverage Index and the commonly used soiling quantification methods: (a) Dust density (b) Soiling ratio; and (c) Relative transmittance loss. Red solid lines represent the linear fitting and the colored area refers to the prediction bounds with a confidence of 90%. (For interpretation of the references to colour in this figure legend, the reader is referred to the web version of this article.)

Table 2

Statistic metrics of the correlations between SCI and conventional soiling indicators.

	$d_{\text{dust}} \text{ vs } \text{SCI}$	$\text{SR vs } \text{SCI}$	$\tau_l \text{ vs } \text{SCI}$
RMSE	0.1790	0.9243	2.8869
MSE	0.0321	0.8544	8.3342
MAE	0.1386	0.8429	2.0433
r^2	0.9554	0.9984	0.9912

Surface coverage index model validation

A detailed analysis was carried out to explore the correlation between the Surface Coverage Index obtained from OSM and the commonly used indicators of soiling. To do so, the initial step involved incorporating the data from the initial conditions to develop semi-empirical models that integrate empirical observations from experimental data with theoretical insights into the mechanisms underlying the soiling phenomenon. These initial conditions correspond to the clean state when no dust particles are present on the surface of the glass coupons and soiling station. This condition is characterized by the following limits: $\lim_{\text{SCI} \rightarrow 0} d_{\text{dust}} = 0$, $\lim_{\text{SCI} \rightarrow 0} \text{SR} = 0$ and $\lim_{\text{SCI} \rightarrow 0} \tau_l = 0$.

The first correlation focuses on the relationship between dust density

and surface coverage index, which is depicted in Fig. 8(a). The outcomes revealed a robust positive linear correlation between these parameters, as indicated by a coefficient of determination $r^2 = 0.95$ and low error showcased in Table. 2. This implies that the response of the surface coverage index to soiling accumulation closely mirrors that of the deposited dust density. Furthermore, this linear fitting proposes a semi-empirical model relating the d_{dust} to the SCI with the following equation:

$$d_{\text{dust}} = \alpha \times \text{SCI} \quad (7)$$

where $\alpha = 0.2645 \text{ g/m}^2$ with 95 % confidence bounds (0.2481, 0.2809). This model gives a good representation of the relationship between deposited dust density and surface coverage index for low to moderate soiling states, which is the most useful range for O&M operators in running power plants, as it is not realistic to leave dust to accumulate for long periods without cleaning. Nevertheless, it is worth mentioning that for high soiling deposition rates, the variation with the surface coverage index may differ from the actual linear fitting as mentioned in [32].

Furthermore, Fig. 8 showcases additional correlations involving the SCI , namely its relationships with both soiling ratio and relative transmittance drop. It is worth noting that to respect the other theoretical limits ($\lim_{\text{SCI} \rightarrow 100} \text{SR} = 100$ and $\lim_{\text{SCI} \rightarrow 100} \tau_l = 100$) representing the state where the surface is completely soiled, the data point translating these limits was added to both SR and τ_l data when plotting the

correlations. Fig. 8(b) and (c) show that the *SCI* exhibited linear positive correlations with both soiling ratio and relative transmittance drop, representing common electrical and optical indicators for soiling monitoring and quantification, respectively. The following semi-empirical model can represent the correlation between the *SCI* and the *SR*:

$$SR = \beta \times SCI - SR_0 \quad (8)$$

where $\beta = 1.01$ with 95 % confidence bounds (0.9867, 1.033), and $SR_0 = -1.377$ with 95 % confidence bounds (-1.968, -0.7866). On the other hand, when examining the other limit $\lim_{SCI \rightarrow 100} SR = 100$, the soiling ratio tends to take a value around 100 % when the surface is fully covered (*SCI* = 100 %). Considering its alignment with the theoretical limits along with a high $r^2 = 0.99$ and the relatively low RMSE of 0.9243, this model fits well with the data demonstrating that the Surface Coverage Index is a good indicator to monitor soiling in a semi-arid climate. Similarly, to *SR*, the relationship between the *SCI* and the transmittance loss can be expressed by the following semi-empirical model:

$$\tau_t = \gamma \times SCI \quad (9)$$

where $\gamma = 1.012$ with 95 % confidence bounds (0.9464, 1.078). Moreover, despite being based on a limited dataset, this correlation remains substantial, boasting an $r^2 = 0.99$. This integral correlation analysis thoroughly explains how the *SCI* aligns with various conventional indicators, emphasizing its effectiveness in quantifying soiling.

An important observation to highlight is the heightened sensitivity of transmittance to dust accumulation on glass samples –indicated by the high Soiling Coverage Index (*SCI*)– compared to electrical measurements. This means the optical measurements tend to overestimate the impact of soiling. In fact, in the transmittance measurements shown in Fig. 8(c), the data points lie above the trend line, illustrating that the sensitivity of dust coverage is significantly higher when measuring the optical properties of the glass. In contrast, when assessing electrical parameters (specifically, the soiling ratio, *SR*), this sensitivity is notably lower, especially with heavier dust accumulation on the PV modules. In such cases, scattered light can still reach the cells and generate electricity, leading to data points that fall below the fitting line. This difference is further emphasized by the end-of-experiment values: the optical transmittance decreased by 15.19 %, whereas the electrical output (*SR*) declined by only 7.3 %.

Conclusion

This study thoroughly investigated PV soiling monitoring, providing significant insights into the efficiency of the Outdoor Soiling Microscope setup for quantifying soiling in the semi-arid climate of Morocco's mid-south region. The research involved synchronizing OSM exposure with traditional soiling stations and analyzing glass coupon exposure. An extensive analysis of the collected dust, performed at IMDEA Energy, identified prevalent minerals like quartz, calcite, dolomite, chlorite, and muscovite, with quartz being the most common. Further examination using Scanning Electron Microscopy and Energy-Dispersive X-ray spectroscopy revealed a range of particle sizes (0–26 μm) and an elemental composition rich in silicon, sodium, calcium, and carbon, indicating significant optical losses due to fine particles. The analysis of soiling in such dusty conditions showed that after a 2-week exposure without rainfall, dust density reached 2.5 g/m^2 , a soiling ratio of 6.9 %, a relative transmittance loss of 15.19 %, and a surface coverage index (*SCI*) of 9.16 %. Furthermore, the comparison of *SCI* derived from the OSM with other conventional soiling monitoring techniques outputs revealed a robust positive linear correlation. In fact, the *SCI* and deposited dust density relationship showed an r^2 of 0.95, suggesting a semi-empirical model for determining dust density based on *SCI* for low to moderate soiling levels. *SCI* also showed strong linear positive correlations with

dust density ($r^2 = 0.95$) and soiling ratio and transmittance loss (both with $r^2 = 0.99$), leading to semi-empirical models for soiling indicators. These findings underscore the efficacy of the OSM in monitoring soiling on PV panels and propose practical models for assessing soiling in similar environments.

Credit author statement

Maryam MEHDI: Conduct field and laboratory experiments, Data processing, Simulation, writing the original Draft. Ricardo Conceição: Conceptualization, Conduct laboratory experiment, Methodology, Data processing, Simulation, writing the original Draft. Nabil AMMARI: Conduct field experiment, data collection. Ahmed Alami Merrouni: Conceptualization, Experimental Protocol, supervision, Writing - Original Draft. José González-Aguilar: Conceptualization, Methodology, Writing - Original Draft. Mohamed Dahmani: Reading & Editing.

CRediT authorship contribution statement

Maryam Mehdi: Writing – original draft, Validation, Software, Investigation, Data curation, Conceptualization. **Ricardo Conceição:** Writing – original draft, Validation, Software, Methodology, Formal analysis, Data curation, Conceptualization. **Nabil Ammari:** Data curation, Conceptualization. **Ahmed Alami Merrouni:** Writing – original draft, Supervision, Project administration, Methodology, Conceptualization. **José González-Aguilar:** Writing – original draft, Methodology, Formal analysis, Conceptualization. **Mohamed Dahmani:** Writing – review & editing.

Declaration of competing interest

The authors declare that they have no known competing financial interests or personal relationships that could have appeared to influence the work reported in this paper.

Acknowledgements

The authors would like to acknowledge the SoDeCo project for funding this study under the grant number FKZ 01DG20003. Also, authors would like to acknowledge the European Union's Horizon 2020 research and innovation program SFERA-III under grant agreement N° 823802. A special thanks to Green Energy Park for granting the access to the research facility and for the logistical support. RC acknowledges the Program Juan de la Cierva Formación 2020, reference (FJC2020-043159-I), funded by MCIN/AEI/10.13039/501100011033 and by the European Union NextGenerationEU/PRTR, as well as the grant PID2020-119693RB-C31 (HECTOR) funded by MCIN/AEI/10.13039/501100011033.

Data availability

Data will be made available on request.

References

- [1] Ammari N, Mehdi M, Merrouni AA, Gallassi HE, Chaabelasri E, Ghennioui A. Experimental study on the impact of soiling on the modules temperature and performance of two different PV technologies under hot arid climate. *Heliyon* 2022;8(11). <https://doi.org/10.1016/j.heliyon.2022.e11395>.
- [2] Ilse K, Figgis BW, Naumann V, Hagedorn C, Bagdahn J. Fundamentals of soiling processes on photovoltaic modules. *Renew Sustain Energy Rev* 2018;98:239–54. <https://doi.org/10.1016/j.rser.2018.09.015>.
- [3] M. Mehdi, N. Ammari, A. Alami Merrouni, H. El Gallassi, M. Dahmani, and A. Ghennioui, 'An experimental comparative analysis of different PV technologies performance including the influence of hot-arid climatic parameters: Toward a realistic yield assessment for desert locations', *Renewable Energy*, vol. 205, pp. 695–716, Mar. 2023, doi: 10.1016/j.renene.2023.01.082.
- [4] Muñoz-García M-Á, Fouris T, Pilat E. Analysis of the soiling effect under different conditions on different photovoltaic glasses and cells using an indoor soiling chamber. *Renew Energy* 2021;163:1560–8. <https://doi.org/10.1016/j.renene.2020.10.027>.

- [5] Conceicao R, et al. Saharan dust transport to Europe and its impact on photovoltaic performance: A case study of soiling in Portugal. *Sol Energy* 2018;160:94–102.
- [6] Laarabi B, El Baqqal Y, Dahrouch A, Barhdadi A. Deep analysis of soiling effect on glass transmittance of PV modules in seven sites in Morocco. *Energy* 2020;213: 118811. <https://doi.org/10.1016/j.energy.2020.118811>.
- [7] Ilse K, Khan MZ, Voicu N, Naumann V, Hagendorf C, Bagdahn J. Advanced performance testing of anti-soiling coatings – Part I: Sequential laboratory test methodology covering the physics of natural soiling processes. *Sol Energy Mater Sol Cells* 2019;202:110048. <https://doi.org/10.1016/j.solmat.2019.110048>.
- [8] Zaihidee FM, Mekhilef S, Seyedmahmoudian M, Horan B. Dust as an unalterable deteriorative factor affecting PV panel's efficiency: Why and how. *Renew Sustain Energy Rev* 2016;65:1267–78. <https://doi.org/10.1016/j.rser.2016.06.068>.
- [9] Said SAM, Walwil HM. Fundamental studies on dust fouling effects on PV module performance. *Sol Energy* 2014;107:328–37. <https://doi.org/10.1016/j.solener.2014.05.048>.
- [10] Conceição R, González-Aguilar J, Merrouni AA, Romero M. Soiling effect in solar energy conversion systems: a review. *Renew Sustain Energy Rev* 2022;162:112434. <https://doi.org/10.1016/j.rser.2022.112434>.
- [11] B. Figgis, A. Ennaoui, S. Ahzi, and Y. Remond, 'Review of PV soiling measurement methods', in *2016 International Renewable and Sustainable Energy Conference (IRSEC)*, Marrakech: IEEE, Nov. 2016, pp. 176–180. doi: 10.1109/IRSEC.2016.7984027.
- [12] Fernández-Solas Á, Micheli L, Muller M, Almonacid F, Fernández EF. Design, characterization and indoor validation of the optical soiling detector "DUSST". *Sol Energy* 2020;211:1459–68. <https://doi.org/10.1016/j.solener.2020.10.028>.
- [13] Fernández-Solas Á, Micheli L, Almonacid F, Fernández EF. Indoor validation of a multiwavelength measurement approach to estimate soiling losses in photovoltaic modules. *Sol Energy* 2022;241:584–91. <https://doi.org/10.1016/j.solener.2022.06.036>.
- [14] Smestad GP, et al. Modelling photovoltaic soiling losses through optical characterization. *Sci Rep* 2020;10(1):58. <https://doi.org/10.1038/s41598-019-56868-z>.
- [15] Javed W, Guo B. Laboratory calibration of a light scattering soiling sensor. *Sol Energy* 2022;236:569–75. <https://doi.org/10.1016/j.solener.2022.03.039>.
- [16] B. Aïssa, G. Scabbia, B. W. Figgis, J. Garcia Lopez, and V. Bermudez Benito, 'PV-soiling field-assessment of MarsTM optical sensor operating in the harsh desert environment of the state of Qatar', *Solar Energy*, vol. 239, pp. 139–146, Jun. 2022, doi: 10.1016/j.solener.2022.04.064.
- [17] M. Gostein, S. Faullin, K. Miller, J. Schneider, and B. Stueve, 'Mars Soiling SensorTM', in *2018 IEEE 7th World Conference on Photovoltaic Energy Conversion (WCPEC) (A Joint Conference of 45th IEEE PVSC, 28th PVSEC & 34th EU PVSEC)*, Jun. 2018, pp. 3417–3420. doi: 10.1109/PVSC.2018.8547767.
- [18] M. Muller, J. Morse, L. Micheli, F. Almonacid, and E. F. Fernandez, 'Design and Indoor Validation of "DUSST": A Novel Low-Maintenance Soiling Station: Preprint'.
- [19] Muller M, et al. An in-depth field validation of "DUSST": A novel low-maintenance soiling measurement device. *Prog Photovolt Res Appl* 2021;29(8):953–67. <https://doi.org/10.1002/ppp.3415>.
- [20] J. G. Bessa, L. Micheli, F. Almonacid, and E. F. Fernández, 'Monitoring photovoltaic soiling: assessment, challenges, and perspectives of current and potential strategies', *iScience*, vol. 24, no. 3, p. 102165, Mar. 2021, doi: 10.1016/j.isci.2021.102165.
- [21] Kassab AS, Ugaz VM, King MD, Hassan YA. High resolution study of micrometer particle detachment on different surfaces. *Aerosol Sci Tech* 2013;47(4):351–60. <https://doi.org/10.1080/02786826.2012.752789>.
- [22] Biryukov S, Faiman D, Goldfeld A. An optical system for the quantitative study of particulate contamination on solar collector surfaces. *Sol Energy* 1999;66(5): 371–8. [https://doi.org/10.1016/S0038-092X\(99\)00020-1](https://doi.org/10.1016/S0038-092X(99)00020-1).
- [23] Figgis B, Ennaoui A, Guo B, Javed W, Chen E. Outdoor soiling microscope for measuring particle deposition and resuspension. *Sol Energy* 2016;137:158–64. <https://doi.org/10.1016/j.solener.2016.08.015>.
- [24] B. Figgis, 'Investigation of PV soiling and condensation in desert environments via outdoor microscopy'.
- [25] Ilse KK, et al. Comprehensive analysis of soiling and cementation processes on PV modules in Qatar. *Sol Energy Mater Sol Cells* Nov. 2018;186:309–23. <https://doi.org/10.1016/j.solmat.2018.06.051>.
- [26] Figgis B, et al. Investigation of factors affecting condensation on soiled PV modules. *Sol Energy* 2018;159:488–500. <https://doi.org/10.1016/j.solener.2017.10.089>.
- [27] Ratnaparkhi A, Dave D, Valerino M, Bergin M, Ghoroi C. Quantifying the accuracy of optical transmission loss techniques and identifying the best wavelengths for estimating soiling in a field study. *Sol Energy* 2023;252:391–400. <https://doi.org/10.1016/j.solener.2023.02.005>.
- [28] M. Gostein, J. R. Caron, and B. Littmann, 'Measuring soiling losses at utility-scale PV power plants', in *2014 IEEE 40th Photovoltaic Specialist Conference (PVSC)*, Jun. 2014, pp. 0885–0890. doi: 10.1109/PVSC.2014.6925056.
- [29] Figgis B, Ennaoui A, Ahzi S, Rémond Y. Review of PV soiling particle mechanics in desert environments. *Renew Sustain Energy Rev* 2017;76:872–81. <https://doi.org/10.1016/j.rser.2017.03.100>.
- [30] Chen J, Pan G, Ouyang J, Ma J, Fu L, Zhang L. Study on impacts of dust accumulation and rainfall on PV power reduction in East China. *Energy* 2020;194: 116915. <https://doi.org/10.1016/j.energy.2020.116915>.
- [31] Dehghan M, Rashidi S, Waqas A. Modeling of soiling losses in solar energy systems. *Sustainable Energy Technol Assess* 2022;53:102435. <https://doi.org/10.1016/j.seta.2022.102435>.
- [32] H. El Gallassi, A. Alami Merrouni, M. Chourak, and A. Ghennioui, 'Novel technique for soiling measurement on concentrated solar plants using night-time image analysis', *Solar Energy*, vol. 252, pp. 260–271, Mar. 2023, doi: 10.1016/j.solener.2023.01.057.